Effect of Surfactant Concentration on Foam
From Coreflood Experiments to Implicit-Texture Foam-Model Parameters

Jones, Sian; Laskaris, G.; Vincent-Bonnieu, Sebastien; Farajzadeh, Rouhi; Rossen, Bill

DOI
10.1016/j.jiec.2016.03.041

Publication date
2016

Document Version
Accepted author manuscript

Published in
Journal of Industrial and Engineering Chemistry

Effect Of Surfactant Concentration On Foam: From Coreflood Experiments To Implicit-Texture Foam-Model Parameters

S.A. Jones[a,*] and G. Laskaris[a], S. Vincent-Bonnieu[a,b], R. Farajzadeh[a,b] and W.R. Rossen[a]

[a] Delft University of Technology, Delft, Netherlands

[b] Shell Global Solutions International, Rijswijk, Netherlands

* Corresponding author, *E-mail address:* s.a.jones@tudelft.nl

Abstract

We present a comparative study of foam coreflood experiments with various surfactant concentrations. Plots of apparent viscosity vs. injected gas fraction were obtained for surfactant concentrations at the critical micelle concentration and above. Bulk foam stability was measured for all concentrations and compared with coreflood results. There were different responses to surfactant concentration in bulk and in corefloods.

The coreflood results were matched with an Implicit Texture foam model and the dependency of the model parameters on the surfactant concentration is discussed. Fitting the data requires relating the surfactant concentration to the dry-out function or the limiting capillary-pressure.

1. Introduction

Foam is a dispersion of gas bubbles in a continuous liquid phase where bubbles are separated by thin liquid films called lamellae, stabilized by surfactants or nanoparticles [1,2,3]. Foam for Enhanced Oil Recovery (EOR) aims at controlling gas mobility and dealing with phenomena such as gas gravity override, viscous fingering and preferential channeling due to reservoir heterogeneity [4,5]. Despite the fact that active research on foam for EOR has been on the rise, relatively few field or pilot applications have been developed. In the field, foam can be injected by co-injection of gas and surfactant or by surfactant-alternating-gas (SAG) injection. SAG injection, with its large slugs of liquid and gas injected at the maximum allowable pressure, is the preferred approach for field injection to minimize gravity override and time of injection [6].

Surfactant molecules stabilize the liquid films separating the foam bubbles. It is crucial to select the correct surfactant, and the correct surfactant concentration, so as to stabilize the foam in an EOR process. Foam stability is generally investigated with bulk foam and coreflood experiments. When considering the effect of surfactant concentration, there is a large body of work on the effect on bulk foam stability, e.g. [7], however there is significantly less information on the effect of surfactant concentration on behavior in corefloods. Aronson *et al*. [8] studied the disjoining pressure isotherms for two surfactant concentrations, and found that the higher concentration gave a higher disjoining pressure. The solution with higher disjoining pressure, which is indicative of higher limiting capillary pressure, gave foams that had large flow resistance i.e. gave large pressure gradients along the core. Apaydin and Kovscek [9] considered transient flow behavior and gas mobility at a fixed foam quality and found that displacement efficiency decreased and gas mobility increased (*i.e.* the foam became weaker) with decreasing surfactant concentration. They linked this behavior to the limiting capillary pressure, related to the maximum capillary pressure a foam film can withstand, which is higher at higher surfactant concentrations. Farajzadeh *et al.* [10] also reported that higher surfactant concentrations gave higher values of the limiting capillary pressure. Alvarez *et al.* [11] found that the changes in the limiting capillary pressure with surfactant concentration caused changes in the foam quality at which the transition from low quality to high quality (coalescence dominated) foam behavior occurred i.e. higher surfactant concentrations gave foams that were stable to higher foam qualities. Schramm and Green [12] considered the Marangoni surface elasticities for a range of different surfactant concentrations. They showed surface elasticity decreased with increasing surfactant concentration. In parallel they showed that decreasing surface elasticity gave increased mobility reduction. This suggests that increasing surfactant concentration will increase mobility reduction.

Bulk foam experiments are performed in general by sparging gas in a surfactant solution which is not in contact with rock. Although there is no consensus on the link between bulk and coreflood tests, bulk foam experiments can serve to evaluate foam stability with respect to oil and surfactant type [13,14,15], gas composition [16] or temperature [17]. The half-life for foam volume decay in a tube declines dramatically with surfactant concentration below the Critical Micellar Concentration (CMC) [18]. CMC is defined as the surfactant concentration above which the surface tension remains constant. DLVO models [19,20] provide a phenomenological explanation of foam film stability based on the disjoining pressure. Scheludko [21] proposed that the film will be destabilized when the capillary pressure, Pc, is greater than the structural disjoining pressure. The critical disjoining pressure

above which foam films break is believed to be a function of surfactant type and concentration and electrolyte concentration [1]. Khatib *et al*. [22] showed that foam-film stability was related to gas mobility reduction. They observed that foam dramatically coalesces at a specific capillary pressure, called 'limiting capillary pressure', *Pc**, above which foam is unstable. Below *Pc** the foam coalescence decreases and, consequently, foam apparent viscosity increases. The limiting capillary pressure varies with surfactant type and concentration, electrolyte concentration, foam flowrate and porous medium permeability. Aronson *et al.* [8] studied the relation between the "critical" and "limiting" capillary pressures by measuring the disjoining pressure isotherms of the sodium dodecyl sulfate (SDS) solution and the pressure drop obtained by injecting the same solution in a sandpack. Their results showed that the solutions with highest disjoining pressure display the highest pressure drop in the porous medium and thus the largest flow resistance. Moreover, they found that the "limiting" capillary pressure for foam coalescence in porous media is close to the rupture pressure of a single foam film.

Steady state co-injection corefloods can be performed by measuring the pressure drop across the core, maintaining constant total superficial velocity while varying gas and liquid fractional flow [23,24]. This "foam scan" experimental method was chosen for this study. Two regimes can be identified: the "low quality" regime, "quality" referring to gas fractional flow, in which the pressure drop increases with the increase of the gas fraction, and in the "high quality" regime, in which the pressure drop decreases with the increase of gas fraction. In between these two regimes, the pressure drop reaches generally a single maximum value.

In modeling foam, Implicit Texture (IT) models are used in commercial simulators, e.g. STARS [25], which assume that local steady state is attained instantaneously everywhere in the porous medium [10]. For the purpose of this work only IT models are described and used. Foam mobility is modelled by applying a mobility reduction factor (*FM*) to the gas relative permeability (or equivalently by increasing gas apparent viscosity – defined below). The *FM* factor is a product of different functions which account for the effect of different mechanisms that affect foam behavior, e.g. the presence of oil (saturation and composition), surfactant concentration, water saturation and/or non-Newtonian shear effects (see Appendix 2). These functions include a number of parameters. The modeling methods of Boeije and Rossen [26] and a modified version [10,17] of the Ma *et al*. [27] method have been employed to derive values for some of such parameters by fitting models to the constant total velocity foam-scan experimental datasets.

This paper investigates the effect of surfactant concentration on foam in oil-free corefloods, over a wide range of concentrations, from the CMC up to concentrations similar to those used in corefloods, and across the whole range of foam qualities at constant flow rate. Bulk foam tests over the same range of surfactant concentrations were also carried out, and the results correlated with the coreflood behavior. The predictability of the foam model to the variation of surfactant concentration is tested.

2. Methods

2.1. Surfactant Solutions

The surfactants tested were two formulations of Sodium C14-16 Alpha Olefin Sulfonate (AOS) : AOS-1 and AOS-2 (Bioterge AS-40 and Bioterge AS-40K respectively). Solutions were made up either with a 3% NaCl brine (AOS-1), or with a synthetic sea-water (AOS-2). Different brines were used with different surfactants (AS-40 and AS40K) because there was only enough AS-40 available for one series of corefloods. It was decided to conduct the continuing experiments with AS-40K, which had the closest formulation to AS-40. The composition of the sea-water is given in Appendix 1 along with a measure of the salinity, the total dissolved solids (TDS), for both the mixtures. A wide range of surfactant concentrations were tested, from 0.0007 wt.% up to 1.65 wt.%.

2.2. Surface-Tension Measurements

The surface tensions of all the AOS solutions were tested using a microtensiometer, based on a miniaturized Du Noüy-Padday set-up [28]. The probe in this case was an inert metal alloy rod with diameter of 0.51 mm, and the measurements were based on the "maximum pull force technique" i.e. the probe was dipped into the test solution, then the maximum pull force due to the surface tension was measured as the probe was withdrawn from the solution. The advantage of this miniaturized probe technique over a standard ring measurement is that it only required a sample volume of 2 ml. The temperature of the tensiometer could be adjusted via a connected water bath, and tests were carried out at both 23°C (room temperature) and 60°C (coreflood test conditions).

2.3. Bulk Foam Tests

The bulk foam tests were carried out using a FoamScan apparatus [29]. The test section is a cylindrical glass tube with an internal diameter of 3 cm and a length of 40 cm. The top of the tube was loosely covered to minimize evaporation from the foam. A fixed amount (50 ml) of surfactant solution was placed in this glass tube, then nitrogen was sparged through the glass frit at the bottom of the cylinder at a rate of 30 ml/min to produce foam.

The foam volume was monitored optically, using a CCD camera, and the nitrogen injection was stopped when the foam volume reached 100 ml. The foam volume was then recorded as a function of time as the foam decayed. The half-life of the foam, i.e. the time taken for the foam volume to drop to half the initial value, was taken as a good indicator of bulk foam stability [30].

Bulk foam tests were carried out at room temperature and atmospheric pressure for all surfactant concentrations.

2.4. Coreflood Tests

The cores used for these tests were 1 cm in diameter, 17 cm long samples of Bentheimer sandstone (porosity, ϕ, = 0.23). The cores were coated in epoxy resin (effective core diameter after coating was 0.94 cm) and mounted in aluminum core-holders as previously described [14]. Due to their small size and ease of manufacture a fresh core could be used for each surfactant formulation. Permeability was measured for each core.

Because of the very small pore volume of the core (2.71 cm^3) the volume of the experimental set-up (pipes, connectors, etc.) was kept as small as possible, in order to keep dead volume to a minimum. The full experimental set-up is shown in Figure 1.

To generate the foam the surfactant solutions and nitrogen were co-injected from the bottom of the core at a constant total flow rate, q_t, of 0.1 ml/min. This is equivalent to a superficial (Darcy) velocity of 2.4 x 10^{-5} m/s or 6.75 ft/day. Considering the individual flow rates of the surfactant solution, q_{liq}, and the nitrogen, q_{gas}, the foam quality, or gas fraction, f_g can then be defined as:

$$f_g = \frac{q_{gas}}{q_{gas}+q_{liq}} \quad \text{.....(1)}$$

The surfactant solution was injected using a double-piston displacement pump. The core was flooded with multiple pore volumes of each solution prior to the start of foam tests to ensure that adsorption in the core had no effect on the steady-state behavior for the low concentration solutions.

The nitrogen gas was supplied from a cylinder, at a pressure of 60 bar, to the mass-flow controller. All the experiments were carried out with a back-pressure of 20 bar. The back-pressure regulator used was a locally modified dome-loaded back-pressure regulator with a dead volume of approximately 1 ml.

Pressure measurements were made using four absolute pressure transducers – *P1* was tapped into the input line at the bottom of the core, *P2* and *P3* were connected to two taps in the core (Figure1), and *P4* was located at the outlet of the core, before the back pressure regulator. During each coreflood test the injected foam quality, f_g, was varied and the resultant pressure drop over the core, either the total pressure drop (*P1* - *P4*) or the drop over the central section of the core (*P2* – *P3*), was measured.

Considering the steady-state pressure drop across the core for each foam quality, the apparent viscosity, μ_{app}, of the gas in the presence of foam can be calculated using Darcy's law :

$$\mu_{app} = \frac{k\nabla P}{(u_g+u_l)} \quad \text{.....(2)}$$

where k is the rock permeability, u_l and u_g are the liquid and gas superficial velocities respectively, and ∇P is the average pressure gradient along the core (calculated from the pressure drop over the central section of the core).

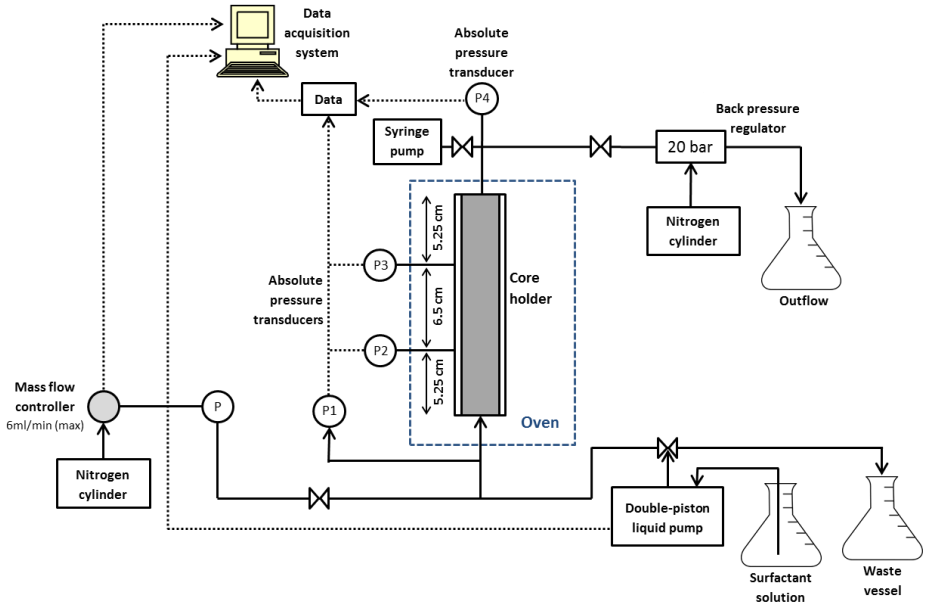

Figure 1: The coreflood experiment set-up. The core was placed in an oven at 60°C, with a back-pressure of 20 bar. The pressure in the system was measured at four points using absolute pressure gauges.

2.5. Modelling

Local-equilibrium models, also known as "implicit texture (IT) models" [10,31], do not explicitly capture the dynamic behavior of foam . In these models, it is customary to consider a non-dimensional mobility reduction factor, FM, which is applied either to the gas phase relative permeability (k_{rg}) or its viscosity (μ_g):

The gas phase relative permeability in the presence of foam, k_{rg}^{f} , can then be defined as:

$$k_{rg}^{f} = k_{rg} \cdot FM \quad \text{.....(3)}$$

In the absence of oil, the IT model relates *FM* to at least three functions of surfactant concentration: F_1, water saturation, F_2, and capillary number, F_5:

$$FM = \frac{1}{1+(fmmob \times F_1 \times F_2 \times F_5)} \quad \text{.....(4)}$$

where *fmmob* is the reference mobility factor, F_1 is a function of the surfactant concentration, F_2 is a function of water saturation and describes coalescence, and F_5 is a function accounting for shear-thinning behavior of foam. Appendix 2 provides a more detailed description of the model functions F_1, F_2 and F_5 and the parameters in those functions. The capillary number, N_{ca}, which represents the balance of viscous forces against the capillary forces, characterized by surface tension, is defined in equation 5:

$$N_{ca} = \frac{\mu_{app} \cdot u}{\sigma_{wg}} \quad \text{.....(5)}$$

where σ_{wg} is the surface tension between the liquid and the gas, μ_{app} is the apparent gas viscosity and u is the total velocity (gas + liquid) within the porous medium. The calculation of the capillary number at different temperatures serves to normalize the value of the apparent gas viscosity with respect to surface tension and velocity [17]. Relative permeabilities for N_2 gas and (surfactant free) brine solution were measured using the unsteady displacement method [32] which allowed the estimation of the Corey parameters, water saturation at residual gas conditions S_{gr}, and connate water saturation, S_{wc}. Values are reported in Table 1. Fitting of the experimental foam-scan data was carried out using an Excel tool in which all five foam parameters (*fmmob*, *fmdry*, *epdry*, *fmcap*, *epcap*) were adjustable. Equal weights were assigned to all experimental data during fitting. The parameters were changed manually so that the model could visually fit the experimental data.

Table 1. Relative permeability (Corey) parameters.

Parameter	Value
S_{wc}	0.25
S_{gr}	0.20
n_w	2.86
n_g	0.70
k_{rw}^0	0.39
k_{rg}^0	0.59

3. Results

3.1. CMC Measurement

The variation of the surface tension with surfactant concentration for solutions of AOS-1 in 3% NaCl and AOS-2 in synthetic sea-water is shown in Figure 2. Measurements were repeated six times for each concentration and the error bars shown give the standard deviation of the values. The CMC was determined by applying the methodology proposed by Mukerjee and Mysels [33]. The data was plotted as a log - linear graph, and trend lines obtained for both the horizontal and downward sections of the curve (not shown here). The point where the horizontal and downward trend lines intersect is taken as the CMC. It was found that the different salinities had a slight effect on the absolute value of the surface tension, but had negligible effect on the CMC. Both AOS-1 in 3% brine and AOS-2 in synthetic sea-water had a CMC of 0.003 wt.% at 23°C and 0.002 wt% at 60°C. This could seem to be in contradiction to previous work that found the CMC decreasing with increasing salinity [34], but in our case, the divalent ions and the total salinity were different, which makes the comparison difficult. Measurements show that surface tension above the CMC of AOS-1 is larger by 1 mN/m than the surface tension of AOS-2 (with divalent ions). Anachkov *et al*. [35] suggest that divalent ions may assist in the adsorption of surfactant molecules at the liquid-air interface, which reduces the surface tension. This is in agreement with our data.

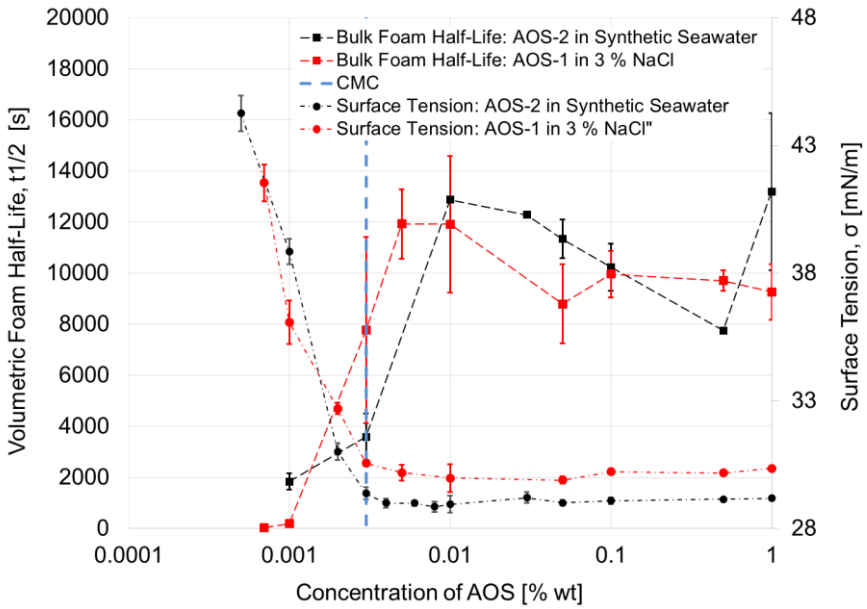

Figure 2: Surface tension and half-life of the bulk foam at 23°C, plotted as a function of surfactant concentration. The surface tension measurements were repeated six times for each concentration, and the bulk foam tests were repeated twice. The error bars indicate the standard deviation in each case.

3.2. Bulk Foam Tests

To quantify the stability of the bulk foam for each surfactant concentration we used the half-life of the foam (Figure 2). Each experiment was repeated twice for each concentration, and the error bars on the graph indicate the standard deviation of the values. We carried out the bulk foam tests at room temperature, instead of 60 °C as in the corefloods, because the bulk-foam setup did not have thermal control. However we measured the CMC at both 23 °C and 60 °C and found the values to be very similar. As the transition from stable to unstable bulk foam depends on the CMC, we suggest that the transition would be similar at 23 °C and 60 °C.

As shown in Figure 2 the stability of the foam increases significantly once the concentration rises above the CMC. This is expected as previous work has described how the greatest effect of the surfactant occurs when a significant concentration of micelles is available, *i.e.* when the concentration is above the CMC and the interfaces are saturated in surfactants [18,36]. The largest increase observed at the 1% concentration was also accompanied by very large error bars, indicating a large difference between the repeat tests. The difference between the two salinities is not significant, although at the CMC, the additional salts in the artificial sea-water appear to slightly reduce stability. It is possible that the Ca in the sea-water can exchange with the sodium on the surfactant molecules and make the surfactant less effective, *i.e.* decrease the effective surfactant concentration, which has greater impact at the low concentrations near the CMC [37].

The slight reduction in foam stability above 0.01% concentration can be attributed to the effect of the micelles on the foam films. DVLO theory provides a theoretical explanation of film stability, but it does not explain the role of micelles in this stability. Lee et al [38]

showed that the presence of micelles can affect the structural disjoining pressure, making it easier for films to rupture when the micelle concentration is significant.

3.3. Coreflood Tests

The effect of surfactant concentration on foam strength for both salinities is shown in Figure 3. As can be seen, the general trend is that as the surfactant concentration decreases, the transition foam quality (*i.e*. the quality at the peak in apparent viscosity), f_g^*, moves to lower values. The corresponding peak apparent viscosity also decreases.

The effect of salinity is noticeable when comparing the results in Figure 3a and Figure 3b. For the tests with 3% NaCl (Figure 3a) there is an obvious "peak" (above the viscosity of the higher concentration solutions) in the apparent viscosity curve near f_g*, but this is not observed in the tests with synthetic sea-water. The "peak" is most noticeable for surfactant concentrations of 0.01% and 0.05%. Similar behaviour has been observed previously by Roerbroeks [39], but as yet we have not found a valid explanation of this behavior.

The overall increase in apparent viscosity observed with sea-water is partly due to the different permeabilities of the two rock samples, as was observed by Kapetas *et al*. [17], who measured increasing foam viscosity with increasing permeability. However, this is partly mitigated by the fact that the calcium ions in the sea-water can exchange with the sodium ions on the surfactant molecules and make the surfactant less effective (or decrease the "effective surfactant concentration") especially at low initial concentrations [40].

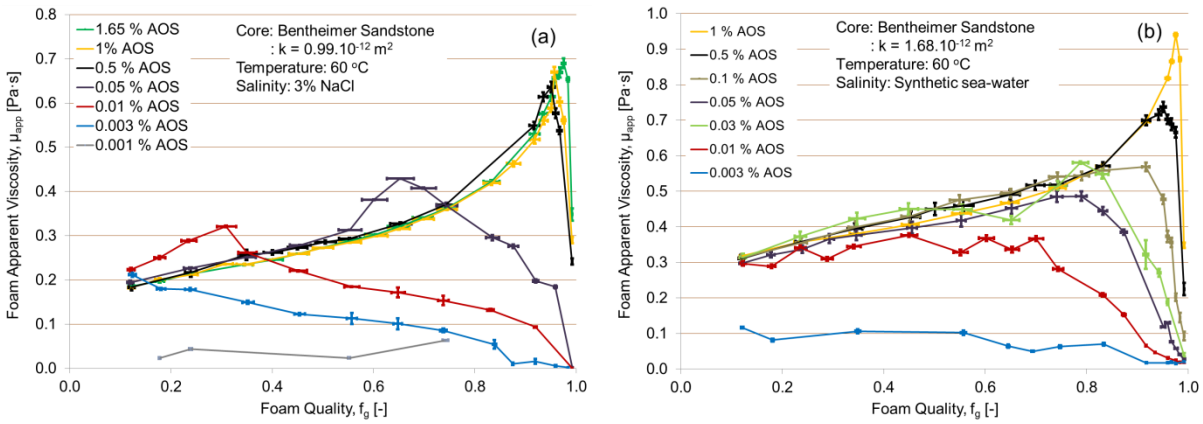

Figure 3: Plots of foam apparent viscosity as a function of injected gas fraction for changing concentrations of AOS in both a) 3% NaCl brine and b) synthetic sea-water

In the bulk foam, the transition in behavior is clearly observed at the CMC (Figure 4). However, in the coreflood the foam strength, characterised by maximum μ_{app}, does not reach a maximum until concentrations well above the CMC. For the AOS-1 results shown (Figure 4) the maximum foam strength is not reached until the concentration is at least 0.5%, which is over 100 times the CMC concentration. There is therefore a significant difference in the response to changes in surfactant concentration between the coreflood and bulk foam.

The movement of surfactant to the interfaces can deplete the concentration in the bulk solution so that there is less surfactant available for new films. If the surface areas of the

bubbles are very high in comparison to the bulk solution, the concentration in the liquid can decrease significantly. It is suggested that the slow increase in foam apparent viscosity above the CMC can be partly due to surfactant depletion in the base solution in each case. In order to estimate this depletion, we consider how much of the surfactant is adsorbed to the gas-water interface as compared to the quantity in the solution [41]. This can be approximated by considering the ratio of the surface area of the bubbles formed with the solution volume in each case (Appendix 3).

It was estimated that the surface area to volume ratio was a factor of 11 higher inside the porous medium of a core as compared to the bulk foam tests, indicating that the surfactant depletion in the solution was a factor of 11 higher in the coreflood tests. The implication of this higher depletion is that the concentration in the solution can be reduced to levels where there is an influence on foam stability. Boos *et al.* [41] observed that even if the initial solution was above the CMC, the concentration in a solution can fall below the CMC as surfactant is adsorbed to the water-gas interfaces as foam is produced. The weaker foam behavior of solutions above the CMC in the coreflood could then be attributed to a greater surfactant depletion of the solution in the core.

It is acknowledged that this is a simplified geometrical consideration of the foam, and ignores any potential effects of geochemistry, rock-fluid interaction, adsorption of surfactant to the rock surface, or the impact of the rate of surfactant transport from bulk to the interfaces (as well as the dynamic effects on the foam in the coreflood, where the films expand and contract when traversing pores), but it goes some way to quantify the difference between the foam in bulk or coreflood.

We therefore expect to see the transition from unstable behavior to stable behavior at a concentration much higher than the CMC in the porous media.

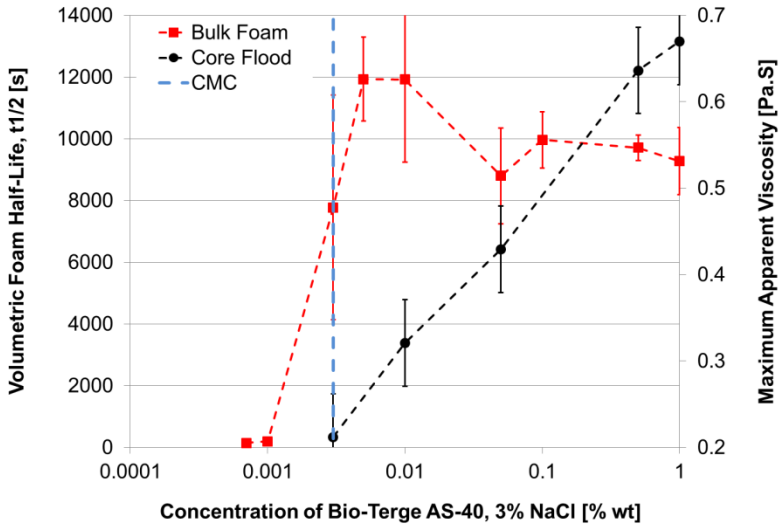

Figure 4: Comparison of the bulk foam and coreflood behaviour as a function of surfactant concentration for the A0S-1 in 3% NaCl.

3.4. Modelling

The foam model equations are presented in Appendix 2. The model was used to interpret the effect of surfactant concentration on the foam mobility. Two approaches were followed to analyze the experimental results. In the first instance, the foam model was employed as originally formulated, meaning the parameter values independent of the concentration are kept constant. In the second case, an extended form of the same model was used –wherein the parameters are all considered functions of surfactant concentration.

(1) In order to investigate the ability of the model to predict the effect of the surfactant concentration, the following analysis was conducted: first, the fitting parameters were determined for the functions *fmmob*, F_1, F_2 and F_5 at the maximum concentration that is supposed to be independent of the surfactant concentration. The set of parameters at the maximum concentration (1 wt%) is the reference case, plotted in Figure 5 (*a* and *b* - red curves). Secondly, the parameters were kept constant, equal to the value obtained at 1wt%, as reported in Table 2 and Table 3, except for the concentration value in the function F_1 (equation B1). Only F_1 is adjusted in order to compare the prediction of the model and the results. The reference fits are shown in Figure 5 (*a* and *b* - red curves). The predictions are represented in Figure 5 (*c, d, e, f* - red curves). The model predictions deviated significantly from the data because the effect of the concentration is only scaling down the apparent viscosity. The model does not account for the change of the transition quality, which shifts to low quality as the concentration decreases. This implies that the foam strength is incorrectly predicted, by a factor of 2 to 4. Consequently, the model examined here does not correctly account for the effect of surfactant concentration on the high-quality regime, i.e. on *fmdry*.

(2) The second approach was to investigate the effect of the concentration on the parameters. In this approach, the model is not used to predict the foam behavior. The data at each concentration was fitted with all parameters. The parameters are reported in Table 2 and Table 3. The results are presented for three concentrations (1 wt%, 0.05 wt% and 0.003 wt%) in Figure 5. Model fitting shows that *fmdry* and *fmmob* decrease with increasing concentration (Figure 6). The dependency of *fmdry* with concentration can be explained by the limiting capillary pressure P_c^* effect. In the IT model, *fmdry* relates to the collapse of the foam at the limiting capillary pressure P_c^* at which the foam collapses [22,42], suggesting that *fmdry* is the water saturation at P_c^*. Water saturation at P_c^* increases by more than 20% when the surfactant concentration decreases to 0.003%. This implies that the foam is less stable at low surfactant concentration. The increase of apparent viscosity with increasing surfactant concentration would suggest that sweep efficiency is also improved. Apaydin and Kovscek [9] showed in their experiments that the overall recovery and the time to gas breakthrough increase as the surfactant concentration increases. At the maximum concentration, *fmdry* (~0.26) is almost equal to the connate water saturation (~0.25) which means that foam is very stable. A similar trend is observed with the AOS -1 and AOS-2, suggesting that the results are consistent. The data was fitted without adjusting *epdry*, as it is not expected that *epdry* varies with the surfactant concentration. Further study of the transition at f_g^* could clarify this effect.

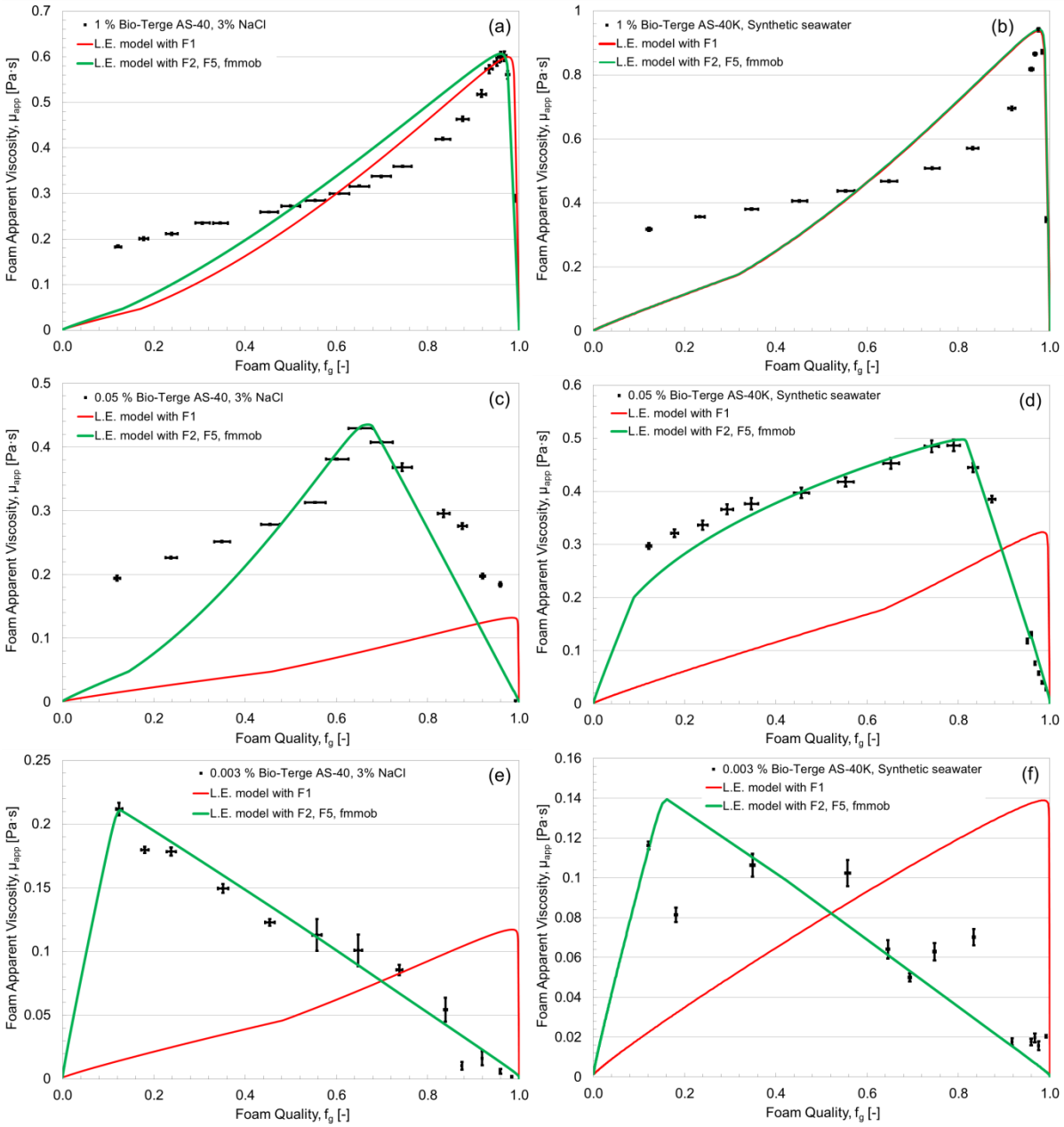

Figure 5: Apparent viscosity of the foam versus the foam quality for constant velocity at three surfactant concentrations : 1% (a,b), 0.5% (c,d) and 0.003% (e,f). Two coreflood experiments are represented on the left (a,c,e) Bentheimer with AOS-1 and on the right (b,c,f) Bentheimer rock with AOS-2. The black crosses represent the experimental data and the standard error. The red curves represent the models fits adjusting only the F_1 function. The green curves represent the model fits adjusting the parameters *fmmob* and the functions F_2 and F_5.

Table 2: Fitting parameters of the IT model matching of the core A results with the F_2 and the F_5 functions and *fmmob*

Concentration	0.001 %	0.003 %	0.01 %	0.03 %	0.05 %	0.1 %	0.5 %	1 .0 %	1.65 %
fmmob	42000	39600	94000	**	6500	**	6100	7000	5940
epdry	5000	5000	5000	**	5000	**	5000	5000	5000

fmdry	0.406	0.3424	0.3233	**	0.300	**	0.270	0.268	0.263
fmcap	0	0	0.0004	**	0.0002	**	0.0002	0.0002	0.0002
epcap	0	0	1.1	**	-0.40	**	-0.38	-0.31	-0.4

Table 3: Fitting parameters of the IT model matching of the core B results with the F_2 and the F_5 functions and *fmmob*

Concentration	0.001 %	0.003 %	0.01 %	0.03 %	0.05 %	0.1 %	0.5 %	1.0 %	1.65 %
fmmob	**	20000	98000	84300	49000	55000	10100	12200	**
epdry	**	5000	5000	5000	5000	5000	5000	5000	**
fmdry	**	0.3552	0.3032	0.2843	0.2892	0.2752	0.267	0.261	**
fmcap	**	0	0.0008	0.0008	0.0009	0.0009	0.0007	0.0008	**
epcap	**	0	2.2	1.3	1.3	1.2	-0.4	-0.4	**

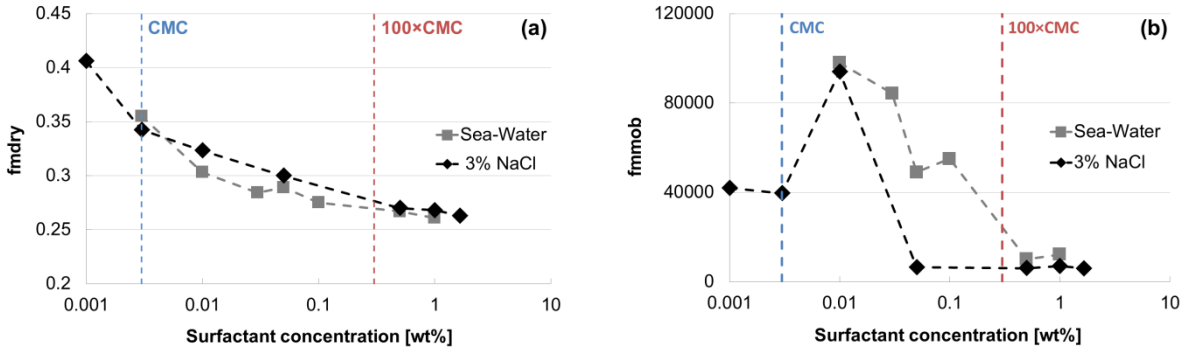

Figure 6: Dependency of the parameters (a) *fmdry* and (b) *fmmob* on the surfactant concentration. The parameters are obtained from the corefloods with both AOS-1 in 3% NaCl and AOS-2 in synthetic sea-water

4. Conclusions

This study presents the bulk foam and coreflood experiments at different surfactant concentrations for two AOS formulations with different salinities. For the rocks and the surfactant type used in the experiments and under our experimental conditions the following conclusions can be drawn. The foam stability in bulk has a transition at the CMC, however in the coreflood experiments, the foam stability shows only a gradual increase with increasing surfactant concentration. It is suggested that this disparity is related to surfactant depletion from the bulk aqueous liquid to the gas/water interfaces of the foam lamellae, as quantified by the ratio S_b/V_s, within the solution, and effect which is significantly stronger in porous media than in the bulk foam. The surfactant molecules moving to the surface during foam generation reduced the available surfactant in the solution, thus reducing the resultant surfactant concentration.

An IT model was used to fit the coreflood data at the highest concentrations, and then the model parameters were used to predict the results at lower concentrations. This model was not able to predict the effect of the concentration on the foam apparent viscosity. In a second approach the model was extended such that five foam parameters vary with surfactant concentration. The results for all concentrations were fitted with all the foam parameters, and the results showed that the effect of the concentration is mostly on *fmdry*, which can be explained by the effect of the surfactant concentration on the limiting capillary pressure, P_c^*. These findings argue in favor of extending IT foam models so that the value of *Pc**can vary with surfactant concentration.

Acknowledgements

We gratefully acknowledge Shell GSI for granting the permission to publish this work. We also thank Dr Reza Bagheri for careful reading of the draft of the manuscript and the technical support of Michiel Slob at the Laboratory Geoscience and Engineering of Delft University of Technology.

5. Nomenclature

SI units are assumed for all parameters used in calculations.

A	Cross-sectional area of core sample
c	Surfactant concentration
$Csurf$	Surfactant concentration for the IT model
$epcap$	Foam parameter controlling shear thinning
$epdry$	Foam parameter controlling abruptness of foam collapse with respect to water saturation
$epsurf$	Foam parameter controlling abruptness of foam collapse with respect to surfactant concentration
$F1$	Function of surfactant concentration Csurf on foam properties
$F2$	Function of water saturation on foam properties
$F3$	Function of oil saturation
$F4$	Function of gas velocity
$F5$	Function of capillary number
$F6$	Function of critical capillary number
FM	Mobility reduction factor
$fmcap$	Foam parameter assumed equal to smallest expected capillary number
$fmmob$	Reference mobility reduction factor
$fmdry$	Critical water saturation at which foam collapses
$fmsurf$	Critical surfactant concentration below which the foam collapse
f_g	Gas fraction or foam quality
f_g^*	Transition foam quality
k	Measured permeability of rock sample to surfactant solution
k_{rg}	Relative permeability of gaseous phase in absence of foam
k_{rg}^0	End-point relative permeability of gaseous phase
k_{rw}^0	End-point relative permeability of aqueous phase
N_{ca}	Capillary number
n_b	Number of bubbles
n_g	Exponent in krg curve
n_w	Exponent in krw curve
P_c^*	Limiting capillary pressure
q_t	Total volumetric flow rate
q_{gas}	Gas volumetric flow rate
q_{liq}	Liquid volumetric flow rate
r	Radius of bubble
S_b	Total surface area of bubbles
S_{gr}	Residual gas saturation
S_w	Water saturation
S_w^*	Water saturation at Pc*
S_{wc}	Connate water saturation
u	Darcy velocity
Vs	Volume of surfactant solution
ϕ	Porosity
μ_g	Viscosity of gas (cP)
μ_w	Viscosity of water (cP)
μ_{app}	Average apparent foam viscosity for middle core section (cP)
σ_{wg}	Surface tension (mN/m)

References

[1] D. Exerowa, P.M. Kruglyakov, Foam and Foam Films: Theory, Experiment, Application. Elsevier, 1997

[2] A. Cervantes Martinez, E. Rio, G. Delon, A. Saint-Jalmes, D. Langevin, B.P. Binks, Soft Matter 4 (2008) 1531-1535.

[3] A.A.Eftekhari, R. Krastev, R. Farajzadeh, Ind. Eng. Chem. Res. 54 (2015) 12482–12491.

[4] J.X. Shi, W.R. Rossen, SPE-35166-MS (1996).

[5] L.L. Schramm, Foams: Fundamentals and Applications in the Petroleum Industry (Vol. 242), American Chemical Society, 1994.

[6] D. Shan, W.R. Rossen, SPE J. 9 (2004) 132–150.

[7] D. Langevin, Adv. Colloid Interface Sci. 88 (2000) 209-222.

[8] A.S. Aronson, V. Bergeron, M.E. Fagan, C.J. Radke, Colloid Surface A. 83 (1994) 109-120.

[9] O.G. Apaydin, A.R. Kovscek, Transport Porous Med. 43 (2001) 511–536.

[10] R. Farajzadeh, M. Lotfollahi, A.A. Eftekhari, W.R. Rossen, G.J. Hirasaki, Energ. Fuel. 29 (2015) 3011–3018.

[11] J.M. Alvarez, H.J. Rivas, W.R. Rossen, SPE J. 6 (2001): 3–6.

[12] L.L. Schramm, W.H.F. Green, Colloid Surface A. 94 (1995) 13-28.

[13] A.K. Vikingstad, A. Skauge, H. Høiland, M. Aarra, Colloid Surface A. 260 (2005) 189-198.

[14] S.A. Jones, V. van der Bent, R. Farajzadeh, W.R. Rossen, S. Vincent-Bonnieu, 18th European Symposium on Improved Oil Recovery, EAGE (2015). DOI: 10.3997/2214-4609.201412126.

[15] A. Andrianov, R. Farajzadeh, M. Mahamoodi Nick, M. Talanana, P.L.J. Zitha, Ind. Eng. Chem. Res. 51 (2012) 2214–2226.

[16] R. Farajzadeh, S. Vincent-Bonnieu, N. Bourada, J. Soft Matter (2014) 145352.

[17] L. Kapetas, S. Vincent-Bonnieu, R. Farajzadeh, A.A. Eftekhari, S.R. Mohd-Shafian, R.Z. Kamarul Bahrim, W.R. Rossen, 18th European Symposium on Improved Oil Recovery, EAGE (2015). DOI: 10.3997/2214-4609.201412124.

[18] L.L. Schramm, Surfactants: Fundamentals and Applications in the Petroleum Industry, Cambridge University Press, 2000.

[19] B. V. Derjaguin, L. Landau, Acta Phys-Chim. USSR. 14 (1941) 633-652.

[20] E. J. Verwey, J. Th. G. Overbeek, Theory of the Stability of Lyophobic Colloids, Elsevier, Amsterdam, 1948.

[21] B.P. Radoev, A.D. Scheludko, E.D. Manev, J.Coll.Interface Sci., 95 (1983)254-265.

[22] Z.I. Khatib, , G.J. Hirasaki, A.H. Falls, SPE Reservoir Eng. 3 (1988) 919–926.

[23] K. Ma, J.L. Lopez-Salinas, M.C. Puerto, C.A. Miller, S.L. Biswal, G.J. Hirasaki, Energ. Fuel. 27 (2013) 2363-2375.

[24] A. Moradi-Araghi, E.L. Johnston, D.R. Zornes, K.J. Harpole, SPE-37218-MS (1997) 81-90.

[25] L. Cheng, A.B. Reme, D. Shan, D.A. Coombe, W.R. Rossen, SPE-59287-MS (2000).

[26] C.S. Boeije, W.R. Rossen, SPE Res. Eval. & Eng. 18 (2015) 264-272.

[27] K. Ma, G. Ren, K. Mateen, D. Morel, P. Cordelier, SPE J. 20 (2015) 453–470.

[28] Kibron, Tensionmeters, http://www.kibron.com/products/tensiometers/ez-pi-plus (Accessed 22 January 2016).

[29] Teclis Instruments, Foamscan, http://www.teclis-instruments.com/index.php/en/offer/products/foam-analyzer/foamscan (Accessed 22 January 2016).

[30] R. Aveyard, B.P. Binks, P.D.I. Fletcher, T.G. Peck, C.E. Rutherford, Adv Colloid Interfac. 48 (1994) 93–120.

[31] M. Lotfollahi, R. Farajzadeh, M. Delshad, A.J. Varavei, W.R. Rossen, SPE-179808 (2016).

[32] E.F. Johnson, D.P. Bossler, V.O. Naumann, Petroleum Transactions, AIME, 216 (1959) 370-372. SPE-1023-G.

[33] P. Mukerjee, K.J. Mysels, Critical Micelle Concentrations of Aqueous Surfactant Systems, National Bureau of Standards, 1970.

[34] R. Farajzadeh, R. Krastev, P.L.J. Zitha, Colloid Surface A. 324 (2008) 35-40.

[35] S.E. Anachkov, S. Tcholakova, D.T. Dimitrova, N.D. Denkov, N. Subrahmaniam, P. Bhunia, Colloid Surface A. 466 (2015) 18–27.

[36] R.K. Prud'homme, S.A. Khan, Foams, Theory, Measurements, and Applications, Surfactant Science series (Vol. 57) Marcel Dekker, New York, 1997.

[37] G. Hirasaki, SPE J. 22 (1982) 181-192.

[38] J. Lee, A. Nikolov, D. Wasan, J Colloid Interf Sci. 415 (2014) 18-25.

[39] J. Roerbroeks, Master's thesis, TU Delft, Delft, The Netherlands, 2014

[40] M.J. Schwuger, E.J. Smulders, Inorganic Builders, in Detergency: Theory and Technology, edited by G. Cutler and E. Kissa, Marcel Dekker, New York, 1987.

[41] J. Boos, W. Drenckhan, C. Stubenrauch, Langmuir 28 (2012) 9303–9310.

[42] Z. Zhou, W.R. Rossen, SPE Adv. Tech. Series 3 (1995) 154–162.

[43] A.A. Eftekhari, R. Farajzadeh, SPE-179647-MS (2016)

Appendix 1. Sea-Water Composition

A seven-salt synthetic sea-water was used for the tests here. The components of the sea-water and their proportions are shown below (Table A-1). The total dissolved solids (TDS) for this sea-water was 35.2g/liter, slightly higher than the 30g/liter for the 3% NaCl brine solution.

Table A-1: The components of the seven-salt synthetic sea-water, with their respective quantities.

Salt Type	Quantity (g / liter)
NaCl	24.501
KCl	0.673
$MgCl_2$. $6H_2O$	10.150
$CaCl_2$. $2H_2O$	1.449
$SrCl_2$. 6 H_2O	0.015
Na_2SO_4 . $10H_2O$	8.717
$NaHCO_3$	0.328

To ensure there were no solubility problems, the solution was made by adding the salts in the following order: 1) Sodium bicarbonate, 2) Calcium chloride, 3) Magnesium chloride, 4) Strontium chloride, 5) Sodium sulphate decahydrate, 6) Potassium chloride, 7) Sodium chloride. .

Appendix 2. IT model

The IT model used in this study is described by Cheng *et al.* [25] and Boeije and Rossen [26], and *fmmob* refers to the gas mobility-reduction factor for wet foams. It corresponds to the maximum mobility reduction. The functions F_1-F_6 are constrained to values less than or equal to 1, so that each function can only reduce the gas mobility-reduction factor, i.e. increase gas mobility. The functions model the effect of surfactant concentration C_{surf} on foam properties (F_1), effect of water saturation on foam properties (F_2), oil saturation (F_3), critical capillary number (F_4), capillary number (F_5) and the critical mole fraction (F_6). In the present work, only F_1, F_2 and F_5 are considered, and defined with equations B1, B2 and B3, respectively:

$$F_1 = \left(\frac{C_{surf}}{fmsurf}\right)^{\text{epsurf}} \quad \text{(B1)}$$

$$F_2 = 0.5 + \frac{\arctan\left(epdry\left(S_w - fmdry\right)\right)}{\pi} \quad \text{(B2)}$$

$$F_5 = \left(\frac{fmcap}{N_{ca}}\right)^{epcap} \quad \text{(B3)}$$

Thus the foam model we use contains seven parameters, namely *fmsurf, epsurf, fmmob, fmdry, epdry, fmcap and epcap*. *epdry* controls the sharpness of the transition from low to high quality. Higher *epdry* generates sharper transition. If the transition between regimes is abrupt, the parameter *fmdry* is equal to S_w^*, the water saturation at the limiting capillary pressure P_c*, i.e. the water saturation at which foam collapses [42].

fmcap represents the lowest capillary number expected in the simulation and below this value shear thinning behavior is not expected. Thus *fmcap* is not considered a foam parameter per se. Parameter *epcap* controls the significance of shear thinning; the larger it is, the stronger the shearing thinning behavior becomes.

Appendix 3. Estimation of the relative surfactant depletion

The estimation of the relative surfactant depletion in the aqueous phase for the bulk foam and coreflood tests is based on the work of Boos *et al.* [41]. They considered the change in surfactant concentration, Δc, and showed that:

$$\Delta c = \frac{1}{V_s N_A}\frac{S_b}{A_{mol}},$$

where S_b is the total surface area of the foam, V_s is the volume of the aqueous surfactant solution, N_A is Avogadro's number (6.02×10^{23} mol^{-1}) and A_{mol} is the area per molecule. If we assume that all foam in the core is made up of spherical bubbles, we can make the following estimations of Δc for the bulk foam and the coreflood.

A3.1. Calculation of Δc for the bulk foam

The volume of solution, V_s, is 50 cm^3

To calculate the surface area of the bubbles, we estimate an average liquid fraction of 10%, giving 90 cm^3 of gas in our 100 cm^3 of foam.

The number of bubbles, n_b, is then equal to the volume of gas divided by the bubble volume, *i.e.*

$$n_b = \frac{9\times10^{-5}}{\frac{4}{3}\pi r^3}$$

where r is the radius of the bubble.

The total surface area of the bubbles is then equal to $S_b = n_b . 4\pi r^2 = \frac{2.7\times10^{-4}}{r}$ m^2

With an approximate bubble radius of 5×10^{-4} m in the bulk foam (estimated from photographs of the foam), $S_b = 0.54$ m^2. The polydispersity of the bubbles was not included in this calculation. Taking $N_A = 6.02 \times 10^{23}$, and the area per molecule as 4×10^{-19} m^2 [ref], we find

$$\Delta c = \frac{S_b}{V_s}.\frac{1}{N_A A_{mol}} = \frac{0.54}{5\times10^{-5}}.\frac{1}{6.02\times10^{23}\times4\times10^{-19}} = \mathbf{0.045\ mol/m^3}$$

This depletion is less than the cmc of the solution (0.104 mol/m^3), indicating that the surfactant depletion will only have any significant effect on foam stability at surfactant concentrations at, and just above, the cmc.

A3.2. Calculation of Δc for foam in the core

The volume of solution, V_s, is calculated from the water saturation in the core, S_w, (estimated from measurements by Eftekhari and Farajzadeh [43]).

ie $V_s = S_w.\ Pore\ Volume = 0.2 \times 2.7 = 0.54$

The number of bubbles is again equal to the volume of gas in the core divided by the bubble volume.

$$n_b = \frac{(0.8 \times 2.7)}{\frac{4}{3}\pi r^2}$$

The total surface area of the bubble is then equal to $S_b = n_b . 4\pi r^2 = \frac{6.48}{r}$

Assuming a bubble radius determined by an average pore size of 200μm, we find

$$S_b = \frac{6.48 \times 10^{-6}}{100 \times 10^{-6}} = 0.0648 \text{ m}^2$$

And therefore,

$$\Delta c = \frac{S_b}{V_s} . \frac{1}{N_A A_{mol}} = \frac{0.0648}{5.4 \times 10^{-7}} . \frac{1}{6.02 \times 10^{23} . 5 \times 10^{-19}} = \mathbf{0.498\ mol/m^3}$$

This depletion is a factor of 5 higher than the cmc of the solution (0.104 mol/m^3). This would indicate that it is not possible to form a strong foam in a core-flood until the surfactant concentration is at least 6 times the cmc. For surfactant solutions with concentrations less than 6 times the cmc, surfactant depletion will stongly impact foam strength.